Title
Challenges in calculating the bandgap of triazine-based carbon nitride structures

Journal
Journal of Materials Chemistry A, 5(10)

ISSN
2050-7488

Authors
Steinmann, Stephan N
Melissen, Sigismund TAG
Le Bahers, Tangui
et al.

Publication Date
2017

DOI
10.1039/c6ta08939a

Peer reviewed

Challenges in Calculating the Bandgap of Triazine-Based Carbon Nitride Structures†

Stephan N. Steinmann,‡ Sigismund T.A.G. Melissen,‡§, Tangui Le Bahers and Philippe Sautet¶

Received 30th May 2016, Accepted Xth XXXXXXXXX 20XX

First published on the web Xth XXXXXXXXXX 200X

DOI: 10.1039/b000000x

Graphitic carbon nitrides form a popular family of materials, particularly as photoharvesters in photocatalytic water splitting cells. Recently, relatively ordered *g*-C_3N_4 and *g*-$C_6N_9H_3$ were characterized by X-Ray diffraction and their ability to photogenerate excitons was subsequently estimated using Density Functional Theory. In this study, the ability of triazine-based *g*-C_3N_4 and *g*-$C_6N_9H_3$ to photogenerate excitons was studied using self-consistent GW computations followed by solving the Bethe-Salpeter Equation (BSE). We will use the prefix "gt-" to refer to these *g*raphitic, *t*riazine-based structures. In particular, monolayers, bilayers and 3D-periodic systems were characterized. The predicted optical band gaps are in the order of 1 eV higher than the experimentally measured ones, which is explained by a combination of shortcomings in the adopted model, small defects in the experimentally obtained structure and the particular nature of the experimental determination of the band gap.

1 Introduction

The first representatives of the graphitic carbon nitrides (CN) based family were synthesized in the 1990s.[1,2] They have a graphite-based structure made of 2D CN covalent layers with the general formula of *g*-$C_xN_yH_z$ held together by Van der Waals interactions. Hence, just like graphite, CNs can be exfoliated to produce nano-materials.[3,4] Their applications[5] have benefited from the large and recent development of the graphite and graphene fields of research. Now, CN materials are investigated for applications in scientific and technological areas including supercapacitors,[6,7] catalysis,[8,9] photocatalysis[10–12] and bio-imaging.[13] For example considerable catalytic activity for Friedel-Crafts (FC)[14] and FC-type[15] reactions – avoiding the waste products created with the commonly used[16] FC catalyst $AlCl_3$ – were reported. Due to the optical gap of about 2.7 eV, the use of CNs in photocatalysis and more precisely in water splitting is probably the most investigated application.[10] From an electronic point of view, the properties of CNs are intermediate between polymeric and inorganic semiconductors.

These characteristics and promising applications explain the large interest of the community for these materials but also the challenges encoutered in their development and their understanding. Quantum chemistry, in particular Density Functional Theory (DFT),[17] appears to be a powerful tool to support experimentalists in the understanding of these materials.[18–20] Unfortunately, also from the quantum mechanical point of view, CN-based materials are challenging systems that push DFT to its limits. First of all, the experimental characterization is often insufficient to build atomistic models. Additionally, capturing the dispersion interactions accurately is challenging and, last but not least, DFT has the tendency to overly delocalize the exciton.[21,22] In this manuscript, the focus will be on the computation of the band gap of the materials. The localized nature of the exciton implies a strong electron-hole interaction, which in turn makes calculating the optical band gap by the difference in energy between the bottom of the conduction band and the top of the valence band (denoted $\boldsymbol{E}_g^{el}$ for electronic band gap) inaccurate.[23] Instead, the exciton binding energy (denoted $\boldsymbol{E}_b$) needs to be included even for qualitative discussions. The following equation, including the experimentally more accessible optical band gap $\boldsymbol{E}_g^{opt}$, summarizes the most important quantities:[24]

$$\boldsymbol{E}_g^{opt} = \boldsymbol{E}_g^{el} - \boldsymbol{E}_b \quad (1)$$

† Electronic Supplementary Information (ESI) available: (1) newly optimized 3D and 2D structures are reported in POSCAR-format (2) Tables and Figures detailing the convergence tests, dielectric responses and system-sensitive computational settings. See DOI: 10.1039/b000000x/

Univ Lyon, École Normale Supérieure de Lyon, CNRS, Université Lyon 1, Laboratoire de Chimie UMR 5182, 46 Allée d'Italie, F-69364, Lyon, France

‡ These authors contributed equally to this work

§ sigismund.melissen@univ-lyon1.fr

Present address:

Institut Lumière Matière

UMR 5306 Université Lyon 1-CNRS,

Université de Lyon, F-69622, Villeurbanne, France

Fax: +33.4.37.37.26.71, Tel: +33.4.72.43.29.69

¶ philippe.sautet@ens-lyon.fr

Present address:

Department of Chemical and Biomolecular engineering

University of California, Los Angeles

Los Angeles, CA 90095, USA

where the superscript "el" is in reference to the "electronic" band gap (sometimes referred to as the "transport" or "fundamental" gap). Previous studies determined the order of magnitude of the exciton binding energy based on the hydrogenic Wannier-Mott (WM) model[25] or applying G_0W_0 - BSE to planar CN layers.[26] Unfortunately, both of these studies have their shortcomings: the WM model assumes a delocalized exciton. The layers of many CNs are, on the other hand, not planar but highly corrugated due to nitrogen lone pair repulsions.[25] Assuming the 2D WM model, we previously obtained exciton radii of 2.9 and 1.2 Å for *gt*-C_3N_4 and *gt*-$C_6N_9H_3$, respectively,[25] which puts into question the applicability of the WM model. Therefore, we aim herein to combine the best of the two previous studies, *i.e.*, the good structural model[25] with the first-principles approach to exciton binding energies.[26]

In this paper, the photophysical properties of *gt*-$C_6N_9H_3$ and *gt*-C_3N_4 are revisited, applying state of the art GW-Bethe-Salpeter Equations (BSE)[27] computations. Unlike DFT, GW is a first principles many body approach to electron correlation, designed to accurately describe the quasi-particle states and thus the fundamental gap.[28,29] GW has been shown to be reliable for condensed phase systems.[30] The exciton binding energy is, subsequently, obtained from the solution of the BSE, which was found to be reliable even for molecules,[31] which is relevant for the type of material discussed here. Additionally, the hypothetical, perfectly flat *gt*-C_3N_4 structure described in ref. 32 is studied using the same methodology, as well as one and two-layer (1L, 2L) slabs to study the influence of corrugation and exfoliation on the photophysical properties. The three bulk systems studied exhibit A-B-A-B stacking, with *gt*-$C_6N_9H_3$ and flat *gt*-C_3N_4 featuring a hexagonal crystal system (space groups $P\bar{6}m2$ and $P6_3/mcm$ respectively) and corrugated *gt*-C_3N_4 featuring a trigonal crystal system (space group $P3c1$).

GW yields an accurate description of $\boldsymbol{E}_{\boldsymbol{g}}^{el}$ whereas the solution of the BSE yields $\boldsymbol{E}_{\boldsymbol{g}}^{opt}$. In addition to these periodic computations, several molecular computations, including Time Dependent DFT (TD-DFT), were performed to study to what extent the excited state properties of the CNs studied here can be traced back to the particular nature of their monomers (see Fig. 1).

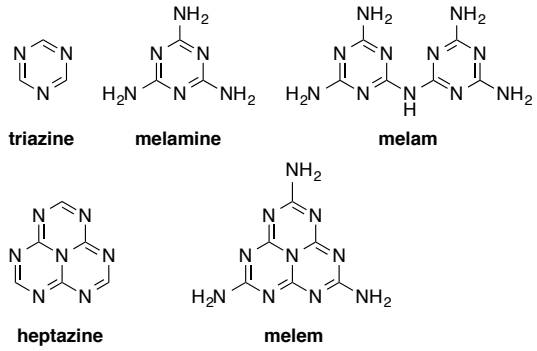

Fig. 1 Organic model molecules serving as a basis for comparison between BSE GW and well established equivalent methods for organic molecules.

2 Computational Details

All newly studied structures were optimized using the CRYSTAL14 quantum chemical suite following the protocol outlined earlier,[25,33] in particular employing the HSE06 functional,[34] a 6-31G(d,p) basis set and a 7×7×3 K-point sampling for the bulk and a 7×7×1 K-point sampling for the mono– and bilayers.[35] Grimme's D2 dispersion correction[36] was used with a scaling factor s_6 of 0.4, to accurately describe the interlayer interactions.[37] For the one and two layer structures the unit cell parameters were kept constant to that of the bulk.

This protocol, and the minor constraint on the 1L and 2L geometries, allow a direct comparison between different structures and to the results obtained in Ref. 25, while only introducing a negligible uncertainty in the present context of advanced electronic structure descriptions.

Electronic structure computations (DFT, GW, BSE) were performed using the Projector Augmented-Wave (PAW) method in the Vienna *Ab Initio* Simulation Package (VASP) 5.3 code,[38] using the pseudopotentials for GW date-marked `28sep2005` (C), `10Apr2007` (N) and `21Apr2008` (H). Both the pure Generalized Gradient Approximation (GGA) functional PBE[39] as well as the HSE06[34] functional were used to compare the fundamental gaps from DFT to scGW.

GW-computations such as those detailed here can be performed on different levels of self-consistency. The entire class of computations will simply be referred to as "GW." "One-shot GW" will be referred to as G_0W_0. Partially self-consistent GW_0 is reported and self-consistent quasi-particle GW,[29,40] in which the eigenvalues and the one electron orbitals are updated for G and W, will be referred to as scGW. All periodic computations include ladder diagrams and vertex corrections based on the inclusion of the non-local exchange-correlation kernel as proposed and implemented in VASP by Shishkin et al.[29] However, the molecular computations were not compatible with this option and hence only include the response-kernel at the level of the direct random phase approximation. Tests on the periodic systems showed that this simplification does not introduce significant changes for the systems under investigation. The full energy dependence of the dielectric function is taken into account (i.e., we do not apply the plasmon-pole approximation), as introduced by Faleev[41] and implemented in VASP by Kresse *et al.*[42] The BSE compu-

tations are based on the corresponding GW computation and carried out in the Tamm-Dancoff approximation as discussed in ref. 43. All GW computations reported herein start from HSE06 orbitals, which have proved to be more valuable for semiconductors than semi-local (GGA) functionals.[18,25,29,44] It must be noted that whereas the WM model naturally includes the vibrational contribution to the dielectric constant, a GW computation does not. In terms of experiments to measure the band gap, the WM results should reproduce a luminescence experiment, whereas a GW should reproduce the band gap as obtained from a UV/Vis diffuse reflectance absorption experiment. In cases of ambiguity, the superscripts $\boldsymbol{v}$ and $\boldsymbol{nv}$ will be added to specifically refer to WM results that include ($\boldsymbol{v}$) and exclude ($\boldsymbol{nv}$) the vibrational contribution.

Our tests showed that the band gaps converged with relatively few bands involved in the GW computations, while the entire spectra requires more sophisticated schemes (*cf.* Fig. S4, SI).[45] The precise number of bands included for the DFT and subsequent GW computations are given in the SI, where additional tests are shown to indicate reasonable convergence (about 0.05 eV). The regular plane wave cut-off energy was set to default (400 eV) and the GW cut-off energy was set to 100 eV, except for the flat 3D-*gt*-C_3N_4, for which a 150 eV cut-off was required, as documented in the SI. Three K-points were used in each periodic direction,[35] i.e, 3×3×1 for mono– and bilayers and 3×3×3 for bulk systems. For the unphysical flat systems, 5 K-points in each periodic direction proved to be necessary to ensure convergence (see SI). Gaussian smearing[46] with $\sigma = 0.01$ eV was used. The electronic convergence criterion for the DFT computations to initialize GW was set to 10^{-7} eV. 8 Å of vacuum were added to the 2D periodic systems. To calculate the optical band gap $\boldsymbol{E_g^{opt}}$ a BSE computation was performed[47] including as many orbitals as necessary to converge the results to about 0.05 eV. The precise number of included orbitals is given in Table S1 of the SI.

Molecular computations at the B2PLYP[48] and Equation Of Motion – Coupled Cluster Singles and Doubles (EOM-CCSD)[49] level of theory are performed with the ORCA package,[50] employing the def2-TZVP[51] and cc-pVDZ[52] basis sets, respectively.

3 Results and Discussion

3.1 Geometry Optimizations

The optimized structures had in-plane lattice constants of 8.56 Å for *gt*-$C_6N_9H_3$, 7.96 Å for corrugated *gt*-C_3N_4 and 4.74 Å for flat *gt*-C_3N_4. To compare the values for the corrugated and flat *gt*-C_3N_4, the latter value needs to be multiplied by $\sqrt{3}$ to account for the different unit cell orientations, which yields 8.21 Å. This is larger than the lattice constant for the corrugated system, since the corrugation naturally contracts the lattice parameter.

Upon imposing planarity in *gt*-C_3N_4, the interlayer distance decreases from 3.38 to 3.11 Å. The *gt*-$C_6N_9H_3$ interlayer distance is equal to 3.26 Å, already obtained in our earlier publication.[25] Overall, these values are in good agreement with earlier reports.[25,53,54]

3.2 Assessment of the GW Protocol

GW and BSE computations in plane-wave codes requires the selection of technical parameters in order to balance computational cost and accuracy. Furthermore, the required settings and expected accuracy depend on the system and properties studied. Here, we are interested in two quantities: the fundamental band gap, as obtained from GW and the lowest excitation energy from solving the BSE. We converged these quantities to a precision of about 0.05 eV with respect to the K-point sampling, the energy cut-off for the response function, the number of bands included and the number of occupied and unoccupied orbitals in the BSE. Overall, we found that these gaps are relatively easy to converge (see computational details and tables in the SI for applied settings). This can be rationalized considering that they are dominated by the splitting between the valence and conduction band. We note in passing, that applying the present protocol to flat *gt*-C_3N_4 and orbitals generated by PBE, leads to very similar results as the ones obtained by Wei and Jacob, although they used a slightly different setup based on orbitals from the local density approximation.[26] In order to assess the quality of GW and BSE@GW for the systems of interest herein, we have investigated the fundamental gap of related small molecules (see Fig. 2) for which reliable *ab initio* data is more accessible. Of course, a molecular system might be more or less sensitive to a given approximation than a solid. However, given that the GW and BSE implementation and numerical settings are tuned for solids, we expect that the accuracy for the molecules could be further improved. For molecules, we compare the fundamental gap to the "integer gap", which is computed as $E(M^+)+E(M^-)-2\times E(M)$, i.e., by doing self-consistent computations for the anion, cation and neutral molecule.[22] This is also the approach taken in a recent GW benchmark study for ionization energies.[55]

The scGW gaps show the same trends as the integer gaps obtained with a reliable double hybrid functional B2PLYP[48,56] (see Fig. 2), justifying the chosen approach. However, the scGW gaps are consistently lower than the DFT gaps, which could be due to a lack of state specific (cation, anion) relaxation of the electronic structure in GW. Compared with the available assessments in the literature,[55,57] the accuracy of GW for molecules is, in general, higher than what is reported herein. On the one hand, these comparisons have only considered the ionization energy and not the fundamental gap

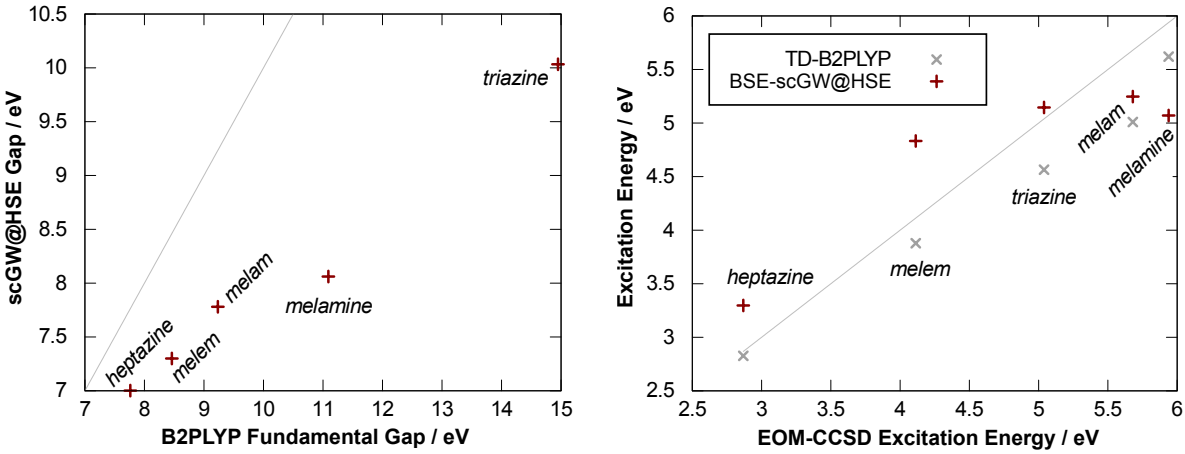

Fig. 2 Parity plot of GW (left) and BSE (right) against B2PLYP (left) and EOM-CCSD (right), two methods with well established accuracy for the quantities in question. As a guide to the eye, the gray line indicates the bisector.

and on the other hand our "benchmark" level (B2PLYP) might yield non-negligible errors for the charged radicals. The second quantity assessed is the lowest electronic excitation. Here, we use EOM-CCSD in a small basis set as the benchmark value and present TD-B2PLYP[58] in a large basis set. Figure S3 also presents data for TD-B2PLYP in the small basis set and BSE@GW computations with more accurate numerical settings. The comparison of EOM-CCSD and TD-B2PLYP in the small basis set demonstrates that TD-B2PLYP describes these excitations very well. Furthermore, in agreement with previous studies,[59] the basis set dependence of these excitations is limited. The BSE results are in rough agreement with EOM-CCSD. However, the relationship is not linear, with a "flattening" observed for the higher energy absorptions: while going from melem to melamine increases the absorption energy by 1.5 eV according to EOM-CCSD, BSE@GW gives almost constant absorptions, with discrepancies larger for melem than for melamine. The accuracy of BSE@GW found herein is somewhat less convincing than what is reported in the literature for molecules.[31,60] Note, however, that the molecules selected for this paper have rather high excitation energies compared to those studied for the benchmark by Jacquemin and co-workers.[31]

Taken the trends for fundamental gap (underestimated) and optical gap (overestimated) together, the molecular computations indicate that GW and BSE@GW might lead to exciton binding energies which are rather low. Nevertheless, the above assessment gives credence to the predictive power of BSE@GW compared to more approximate methods like HSE06 eigenvalues and TD-DFT.

3.3 GW Results for 2D and 3D Systems

In this subsection we discuss the physical content of the results presented, while the next subsection puts them into perspective with earlier computations based on the WM model[25,33] and experimental measurements.[10,32] The present discussion focuses on the scGW data, which we consider the most reliable. Nevertheless, we also comment on the "stability" of the observed trends as a function of the theoretical method. Note that all systems investigated have direct gaps at the Γ-point, except for 3D-*gt*-$C_6N_9H_3$, which features a direct gap best described as $^1/_3\ ^1/_3\ 0 \rightarrow\ ^1/_3\ ^1/_3\ 0$ and 1L and 2L corrugated *gt*-C_3N_4, that have slightly irregular transitions best described as $^1/_9\ ^1/_9\ \rightarrow\ 0\ 0$. An overview of the results is given in Fig. 3. Focusing first on the bulk properties, we observe a significant reduction of the fundamental (-1.5 eV) and optical (-0.9 eV) gap upon increasing the polymerization degree from *gt*-$C_6N_9H_3$ to *gt*-C_3N_4. Since $\boldsymbol{E_g^{el}}$ decreases more significantly than $\boldsymbol{E_g^{opt}}$, $\boldsymbol{E_b}$ decreases as well when increasing the degree of polymerization. This large reduction in the fundamental band gap is difficult to capture for the more approximate DFT levels: with 0.7 and 0.9 eV reductions for PBE and HSE06, the effect is underestimated by 40-50%, demonstrating the importance to use more robust methods in order to obtain quantitative agreement. For instance, G_0W_0 already gives a reduction of 1.3 eV, missing only 15 % of the most reliable estimate.

gt-C_3N_4 that is constrained to remain flat, is a widely studied, but idealized, model. Although in its bulk form it is a high-order saddle point on the potential energy surface, small patches of planar *gt*-C_3N_4 might exist in heterogenous materials.[61,62] The planarity increases the conjugation between the molecular subunits and thus lowers the band gap compared to the corrugated system (Fig. 3c *vs.* Fig. 3b). However, the

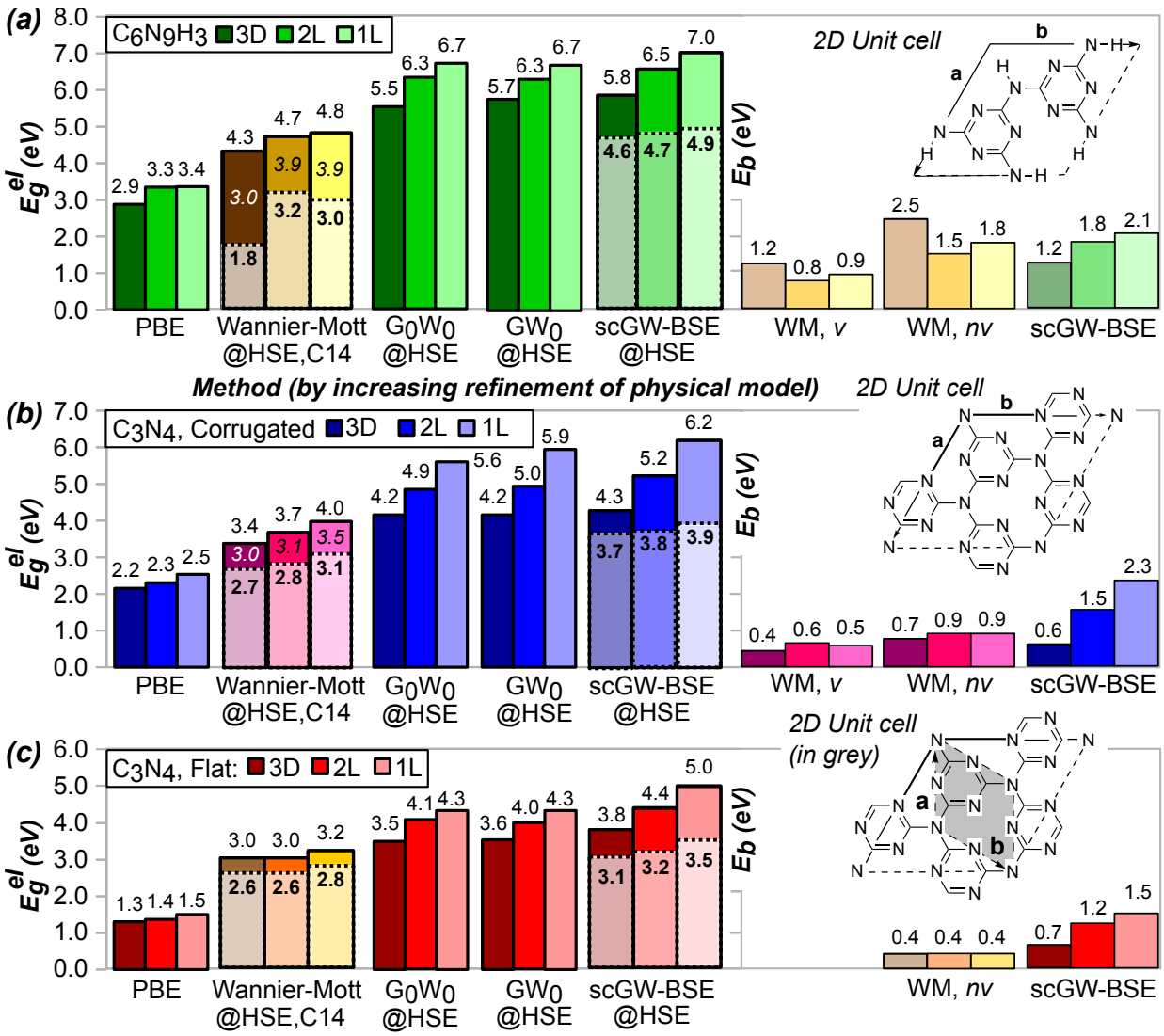

Fig. 3 Summary of most important results presented in this paper, including comparison with earlier work. Electronic band gaps for (a) *gt*-$C_6N_9H_3$, (b) corrugated and (c) flat *gt*-C_3N_4 are reported. The Wannier-Mott analysis using the CRYSTAL14 code reported earlier[25] is depicted in an alternative color scheme. The optical band gaps $\boldsymbol{E_g^{opt,nv}}$ are depicted semi-transparently. For the two physically acceptable structures (*gt*-$C_6N_9H_3$ and corrugated *gt*-C_3N_4) the $\boldsymbol{E_b^{v}}$-corrected band gaps are provided in italics for completion. The WM and scGW–BSE exciton binding energies $\boldsymbol{E_b}$ are provided to the right of the band gaps , with *v* and *nv* denoting vibrationally and not vibrationally corrected respectively. The 2D unit cells for the studied structures are given with lattice vectors **a** and **b**, the flat *gt*-C_3N_4 structure can be described by the cell highlighted in grey, for the corrugated structure the full $\sqrt{3} \times \sqrt{3}$ supercell is needed.

fundamental and optical gap decrease to roughly the same extent, leaving the exciton binding energy unaffected. With the exception of PBE, which clearly overestimates the effect of the conjugation and thus provides a very small fundamental band gap for the planar polymorph, all methods confirm that "planarizing" lowers the band gap by about 0.5 eV.[25,54] This lowering is significant and might indicate that defects and/or doping that are able to stabilize planar patches of fully polymerized CN could tune the adsorption spectrum of these materials.[63]

In a photocatalytic cell the photoharvester requires interfacing with a co-catalyst.[64] The exciton dissociates at this interface and in the case of the hydrogen evolution reaction the electron is transferred to the noble metal co-catalyst that performs the chemical conversion. Since the exciton binding energies of CNs are high ($\gg 10\ k_B T_R$, with k_B Boltzmann's constant and T_R room temperature), spontaneous exciton dissociation at room temperature is unlikely. Therefore a bulk heterojunction-inspired architecture would need to be adopted. One of the possibilities would be to make thin materials, perhaps even limited to several aromatic layers. Furthermore, exfoliation can be an efficient means to increase conductivity and, therefore, photo-electrochemical activity of semiconductors.[65]

Thus motivated, we have systematically investigated the effect of exfoliation on the band gaps. According to our results, the fundamental band gap increases sharply by 1 (*gt*-$C_6N_9H_3$, $\widehat{=} \sim 20\%$) to 2 (*gt*-C_3N_4, $\widehat{=} \sim 30\%$) eV. MoS_2 is another layered material often serving as a reference in this field.[66–68] Its fundamental gap increases from 1.22 to 1.97 eV, $\widehat{=} \sim 60\%$ upon exfoliation according to G_0W_0.[66] Hence, the increase for CNs is smaller in percentages, although higher in absolute terms. Experimentally, MgO is a rather well characterized layered material that exhibits a qualitatively different behavior:[69] the bulk bandgap of 7.6 eV decreases to ∼5 eV upon exfoliation to a bilayer ($\widehat{=} \sim -30\%$). We have investigated the convergence behavior of the band gaps as a function of interlayer distance from 3-14 Å (see Figure S2). In agreement with previous results, the convergence is slow, most likely due to long-ranged electrostatic interactions.[66] Experimentally, such interactions are barely avoidable, since measurements on free standing monolayer are extremely challenging. The K-point convergence of the optical and fundamental gap is, however, quite fast (see Figure S3). Nevertheless, we neither extrapolate to infinitely spaced monolayers, nor exclude that we benefit from some error cancellation, as suggested by Hüser *et al.*[66]

The optical gap remains largely constant from the bulk to the monolayer. As a consequence, the charge separation becomes increasingly more difficult upon exfoliation. These two trends, constant optical gap and increasing fundamental gap upon exfoliation, can be rationalized as follows: The excitation is a local phenomenon in these molecular semiconductors. Consequently, the absorption of light, corresponding to exciton formation, is not affected by the environment and is governed by the properties of the monolayer. Since the excitation dissociation leads to a charge separated state, the long-range polarization of the environment can stabilize the dissociated electron and hole more efficiently in a bulk material than in an isolated monolayer. This explains the increasing exciton binding energy upon exfoliation, in good agreement with previous reports.[70]

In MoS_2 and MgO additional effects come into play. In the case of MoS_2, the difference in bandgap upon exfoliation is governed by the overlap between the sulfur p_z-orbitals and the molybdenum d-orbitals, which is strongly affected by the interlayer distance.[67] In the case of MgO, this difference is mainly governed by the change in coordination number of surface oxygen atoms.[69] This demonstrates how unique each of these three layered materials' optical properties are and that comparisons are not straight forward at all.

Considering only the effect of exfoliation on the fundamental gap, we observe that, very similarly to the effect of further condensation (*gt*-$C_6N_9H_3$ to *gt*-C_3N_4), PBE and HSE06 are completely inadequate to assess the effect: first of all, the fundamental gap increases by only 0.5 eV and second, especially with HSE06, the difference in optical response between *gt*-$C_6N_9H_3$ and *gt*-C_3N_4 is completely lost. This, again, demonstrates the need to go beyond (hybrid) DFT to quantify the optical properties of molecular semiconductors.

3.4 Confronting WM, Experiment and GW

In the previous section we have demonstrated that DFT has limitations in correctly describing all subtle variations of photophysical properties of CN materials related to changing the degree of polymerization or exfoliation. In this section, we discuss the consequences of this on the conclusions in our earlier publication[25] which relied exclusively on the combination of DFT and the WM model.

First of all, the WM model requires the user to declare the dimensionality of the problem: a 2D exciton has a binding energy that is four times the binding energy of the corresponding 3D exciton.[23,71] Since CNs are strongly anisotropic materials and the in-plane physics was assumed to dominate, we mainly discussed the results for the 2D exciton model.[25] For the first principles approach BSE@GW, such an explicit choice for a strictly 2D or a 3D model is not necessary. This allows one to obtain an unbiased estimate, which is highly desirable, since experimental results indicate high exciton mobilities in the z-, or interlayer, direction.[72] However, there is an additional ambiguity when comparing WM with BSE@GW results: conventionally, the WM model includes the "vibrational" contribution to the dielectric constant, which lowers the exciton

binding energy and thus increases the optical band gap. In BSE@GW, in contrast, these effects are not included, since they would either require thermal sampling or excited state geometries. Note, however, that vibrational corrections in the BSE@GW context would affect both the fundamental and the optical band gap, so that the comparison with WM is always skewed. If we compare the exciton binding energies of WM without the vibrational contributions to scGW, we find that the exciton binding energy is overestimated for bulk *gt*-$C_6N_9H_3$, while it is about right for *gt*-C_3N_4. When including the vibrational contributions, the exciton binding energy of 2D-WM and BSE@GW are very close to each other for both bulk systems. Although this can largely be traced back to error cancellation, in both cases the main conclusion holds: first of all, the materials are predominantely two-dimensional (with the third dimension mainly influencing the fundamental gap (*vide supra*), an effect that is somewhat artificially corrected for in the WM model and second the exciton binding energies are very high compared to "standard" inorganic semiconductors. Hence, in applications, the co-catalyst needs to be highly dispersed in order to minimize the exciton diffusion path. Overall, we conclude that for the very basic characteristics the much more economical WM model is sufficient, although we strongly recommend using BSE@GW for detailed studies of the various influences on the photo-physical properties of carbon nitrides. The results further show that increasing the level of self-consistency from G_0W_0 to GW_0 has a similar effect as raising the level of self-consistency from GW_0 to fully self-consistent GW does. This suggests stepwise improvements of the result when introducing stepwise refinements to the chosen method.

An important difficulty when comparing experimental measurements of the optical band gap, $\boldsymbol{E_g^{opt}}$, to computed values comes from the lack of purity of the materials studied. *g*-$C_xN_yH_z$ -based materials are the product of a polymerization process requiring temperatures above those typically employed in organic synthesis, making them more prone to defects than a traditional, polymeric or inorganic semiconductor. Also, material inhomogeneity is a common issue: mixtures of different polymorphs or patches with different x, y and z which average to the nominal composition *g*-$C_xN_yH_z$ are difficult to distinguish experimentally[61] or to purify without special care and advanced techniques. Second, experimentally the optical gap can be determined in different ways, with the two main differences being absorption onset and photoluminescence.[73] To compare with the present computations, absorption onset is clearly the best point of comparison. The fundamental gap is rarely determined at all but would be accessible from electrochemical measurements. We are not aware of any such measurements for carbon nitrides. The most often cited value for the optical (absorption) gap is 2.7 eV.[10] According to BSE@GW, the perfect bulk crystals of *gt*-C_3N_4 and *gt*-$C_6N_9H_3$ yield optical gaps of 3.7 and 4.6 eV, respectively. This is, obviously, quite far from the reported experimental gaps. Having not found any evidence for a systematic overestimation of the optical transitions for related molecules (*vide supra*), we suggest that the experimentally determined value does not correspond to perfect, triazine-based semiconductors. From the results presented herein, we are unable to distinguish between the two most likely explanations for the experimental results: heptazine-based materials and defects, which either increase the planarity of the layers or alter the nature of the elementary units, which in turn show a distinct absorption behavior. In both cases, we can not exclude that a minority site is responsible for the optically measured signal.

4 Conclusions

The band gaps of monolayers, bilayers and 3D periodic, experimentally characterized, triazine-*"(t-)"* based carbon nitrides have been investigated theoretically. In particular, we have presented fundamental and optical band gaps, and thus exciton binding energies at the BSE@GW level of theory. In agreement with previous studies, flat *gt*-C_3N_4 has a lower band gap than corrugated *gt*-C_3N_4 and *gt*-$C_6N_9H_3$ has a higher band gap than both of the others. However, the fundamental band gaps are about 2 eV higher according to scGW than what has been predicted by HSE06. Furthermore, the simple WM model is unable to reliably capture the effect of exfoliation, which leaves the optical gap unchanged, while the fundamental gap increases dramatically. However, in good agreement with the WM model, the exciton binding energy is very high in CNs, making spontaneous exciton dissociation unlikely at room temperature. In comparison with experiment, the computed optical gaps are higher by at least 1 eV for the corrugated *gt*-C_3N_4. Even assuming a conservative error estimate of 0.5 eV for BSE@GW optical gaps, the theoretical gaps are clearly larger than the experimental ones. We tentatively suggest that the experimentally determined gap - itself sensitive to the particular experiment by which it is determined - either corresponds to heptazine-based CNs, patches of material where the C:N ratio is higher than on average, or that a small percentage of nearly planar defects is responsible for the onset of the optical response, which would explain the discrepancy between experiment and scGW for the perfectly crystalline corrugated triazine-based CNs.

Acknowledgments

Funding for this work was provided by the King Abdullah University of Science and Techonology (KAUST), within the framework of Special Academic Partnership Program "Water Splitting" (projects ENS 14.065 and KAUST 1974-02).

The authors gratefully acknowledge Dr. A. Winfer and Dr. I. Shore (KAUST Supercomputing Laboratory), the computational resources provided by *l'Institut du Développement et des Ressources en Informatique Scientifique* (IDRIS, under project x2015080609) of the *Centre National de la Recherche Scientifique (CNRS)* and by the *Pôle Scientifique de Modélisation Numérique (PSMN)* at ENS Lyon.

List of Acronyms

BSE Bethe-Salpeter Equations

DFT Density Functional Theory

EOM-CCSD Equation Of Motion – Coupled Cluster Singles and Doubles

FC Friedel-Crafts

GGA Generalized Gradient Approximation

PAW Projector Augmented-Wave

TD-DFT Time Dependent DFT

VASP Vienna *Ab Initio* Simulation Package

WM Wannier-Mott

References

1 T. Sekine, H. Kanda, Y. Bando, M. Yokoyama and K. Hojou, *J. Mater. Sci. Lett.*, 1990, **9**, 1376–1378.
2 C. Niu, Y. Z. Lu and C. M. Lieber, *Science*, 1993, **261**, 334–337.
3 S. Z. Butler, S. M. Hollen, L. Cao, Y. Cui, J. A. Gupta, H. R. Gutierrez, T. F. Heinz, S. S. Hong, J. Huang, A. F. Ismach, E. Johnston-Halperin, M. Kuno, V. V. Plashnitsa, R. D. Robinson, R. S. Ruoff, S. Salahuddin, J. Shan, L. Shi, M. G. Spencer, M. Terrones, W. Windl and J. E. Goldberger, *ACS Nano*, 2013, **7**, 2898–2926.
4 K. Novoselov, A. K. A.K. Geim, S. V. Morozov, D. Jiang, Y. Zhang, S. V. Dubonos, I. V. Grigorieva and A. A. Firsov, *Science*, 2004, **306**, 666–669.
5 Z. Zhao, Y. Sun and F. Dong, *Nanoscale*, 2015, **7**, 15–37.
6 L. Zhang, M. Ou, H. Yao, Z. Li, D. Qu, F. Liu, J. Wang, J. Wang and Z. Li, *Electrochim. Acta*, 2015, **186**, 292–301.
7 Q. Chen, Y. Zhao, X. Huang, N. Chen and L. Qu, *J. Mater. Chem. A*, 2015, **3**, 6761–6766.
8 J. Zhu, P. Xiao, H. Li and S. A. C. Carabineiro, *ACS Appl. Mater. Interfaces*, 2014, **6**, 16449–16465.
9 Y. Gong, M. Li, H. Li and Y. Wang, *Green Chem.*, 2015, **17**, 715–736.
10 X. Wang, K. Maeda, A. Thomas, K. Takanabe, G. Xin, J. M. Carlsson, K. Domen and M. Antonietti, *Nature Mater.*, 2009, **8**, 76–80.
11 Y. Zheng, J. Liu, J. Liang, M. Jaroniec and S. Z. Qiao, *Energy Environ. Sci.*, 2012, **5**, 6717–6731.
12 J. Zhang, J. Sun, K. Maeda, K. Domen, P. Liu, M. Antonietti, X. Fu and X. Wang, *Energy Environ. Sci.*, 2011, **4**, 675–678.
13 Y. Chen, C. Tan, H. Zhang and L. Wang, *Chem. Soc. Rev.*, 2015, **44**, 2681–2701.
14 A. Thomas, A. Fischer, F. Goettmann, M. Antonietti, J.-O. Müller, R. Schlögl and J. M. Carlsson, *J. Mater. Chem.*, 2008, **18**, 4893–4908.
15 F. Goettmann, A. Thomas and M. Antonietti, *Angew. Chem. Int. Ed.*, 2007, **46**, 2717–2720.
16 (*a*) S. T. A. G. Melissen, V. Tognetti, G. Dupas, J. Jouanneau, G. Lê and L. Joubert, *J. Mol. Model.*, 2013, **19**, 4947–4958; (*b*) S. T. A. G. Melissen, V. Tognetti, G. Dupas, J. Jouanneau, G. Lê and L. Joubert, *J. Mol. Model.*, 2016, **22**, 1–14.
17 W. Kohn and L. J. Sham, *Phys. Rev.*, 1965, **140**, A1133–A1138.
18 T. Le Bahers, M. Rérat and P. Sautet, *J. Phys. Chem. C*, 2014, **118**, 5997–6008.
19 S. T. A. G. Melissen, S. N. Steinmann, T. Le Bahers and P. Sautet, *J. Phys. Chem. C*, 2016, **120**, 24542–24550.
20 (*a*) S. T. A. G. Melissen, F. Labat, P. Sautet and T. Le Bahers, *Phys. Chem. Chem. Phys.*, 2015, **17**, 2199–2209; (*b*) T. A. Kandiel, D. H. Anjum, P. Sautet, T. Le Bahers and K. Takanabe, *J. Mater. Chem. A*, 2015, **3**, 8896–8904; (*c*) T. Le Bahers, S. Haller, T. Le Mercier and P. Barboux, *J. Phys. Chem. C*, 2015, **119**, 17585–17595; (*d*) S. Petit, S. T. A. G. Melissen, L. Duclaux, M. T. Sougrati, T. Le Bahers, P. Sautet, D. Dambournet, O. J. Borkiewicz, C. Laberty-Robert and O. Durupthy, *J. Phys. Chem. C*, 2016, **120**, 24521–24532.
21 B. M. Wong and T. H. Hsieh, *J. Chem. Theory Comput.*, 2010, **6**, 3704–3712.
22 P. Mori-Sánchez, A. J. Cohen and W. Yang, *Phys. Rev. Lett.*, 2008, **100**, 146401.
23 X.-Y. Zhu, Q. Yang and M. Muntwiler, *Acc. Chem. Res.*, 2009, **42**, 1779–1787.
24 B. A. Gregg, *MRS Bull.*, 2005, **30**, 20–22.
25 S. T. A. G. Melissen, T. Le Bahers, S. N. Steinmann and P. Sautet, *J. Phys. Chem. C*, 2015, **119**, 25188–25196.
26 W. Wei and T. Jacob, *Phys. Rev. B*, 2013, **87**, 085202.
27 (*a*) E. E. Salpeter and H. A. Bethe, *Phys. Rev.*, 1951, **84**, 1232–1242; (*b*) L. Hedin, *Phys. Rev.*, 1965, **139**, A796–A823.
28 (*a*) M. Shishkin and G. Kresse, *Phys. Rev. B*, 2006, **74**, 035101; (*b*) M. Shishkin and G. Kresse, *Phys. Rev. B*, 2007, **75**, 235102.
29 M. Shishkin, M. Marsman and G. Kresse, *Phys. Rev. Lett.*, 2007, **99**, 246403.
30 J. Yan, K. W. Jacobsen and K. S. Thygesen, *Phys. Rev. B*, 2012, **86**, 045208.
31 D. Jacquemin, I. Duchemin and X. Blase, *J. Chem. Theory Comput.*, 2015, **11**, 5340–5359.
32 G. Algara-Siller, N. Severin, S. Y. Chong, T. Björkman, R. G. Palgrave, A. Laybourn, M. Antonietti, Y. Z. Khimyak, A. V. Krasheninnikov, J. P. Rabe, U. Kaiser, A. I. Cooper, A. Thomas and M. J. Bojdys, *Angew. Chemie*, 2014, **126**, 7580–7585.
33 M. K. Bhunia, S. Melissen, M. R. Parida, P. Sarawade, J.-M. Basset, D. H. Anjum, O. F. Mohammed, P. Sautet, T. Le Bahers and K. Takanabe, *Chem. Mater.*, 2015, **27**, 8237–8247.
34 (*a*) J. Heyd, G. E. Scuseria and M. Ernzerhof, *J. Chem. Phys.*, 2003, **118**, 8207–8215; (*b*) J. Heyd, G. E. Scuseria and M. Ernzerhof, *J. Chem. Phys.*, 2006, **124**, 219906.
35 H. J. Monkhorst and J. D. Pack, *Phys. Rev. B*, 1976, **13**, 5188–5192.
36 S. Grimme, *J. Comput. Chem.*, 2006, **27**, 1787–1799.
37 V. Wang, R. J. Liu, H. P. He, C. M. Yang and L. Ma, *Solid State Commun.*, 2014, **177**, 74–79.
38 (*a*) G. Kresse and J. Hafner, *Phys. Rev. B*, 1993, **47**, 558–561; (*b*) G. Kresse and J. Hafner, *Phys. Rev. B*, 1994, **49**, 14251–14269; (*c*) G. Kresse and J. Furthmüller, *Comput. Mater. Sci.*, 1996, **6**, 15–50; (*d*) G. Kresse and J. Furthmüller, *Phys. Rev. B*, 1996, **54**, 11169–11186.
39 (*a*) J. P. Perdew, K. Burke and M. Ernzerhof, *Phys. Rev. Lett.*, 1996, **77**, 3865–3868; (*b*) J. P. Perdew, K. Burke and M. Ernzerhof, *Phys. Rev. Lett.*, 1997, **78**, 1396–1396.
40 C. Franchini, A. Sanna, M. Marsman and G. Kresse, *Phys. Rev. B*, 2010, **81**, 085213.
41 S. V. Faleev, M. van Schilfgaarde and T. Kotani, *Phys. Rev. Lett.*, 2004,

93, 126406.
42 G. Kresse, M. Marsman, L. E. Hintzsche and E. Flage-Larsen, *Phys. Rev. B*, 2012, **85**, 045205.
43 T. Sander, E. Maggio and G. Kresse, *Phys. Rev. B*, 2015, **92**, 045209.
44 A. Grüneis, G. Kresse, Y. Hinuma and F. Oba, *Phys. Rev. Lett.*, 2014, **112**, 096401.
45 P. Umari, O. Petrenko, S. Taioli and M. M. De Souza, *J. Chem. Phys.*, 2012, **136**, 181101.
46 M. Methfessel and A. T. Paxton, *Phys. Rev. B*, 1989, **40**, 3616–3621.
47 (*a*) S. Albrecht, L. Reining, R. Del Sole and G. Onida, *Phys. Rev. Lett.*, 1998, **80**, 4510–4513; (*b*) M. Rohlfing and S. G. Louie, *Phys. Rev. Lett.*, 1998, **81**, 2312–2315.
48 S. Grimme, *J. Chem. Phys.*, 2006, **124**, 034108.
49 J. F. Stanton and R. J. Bartlett, *J. Chem. Phys.*, 1993, **98**, 7029–7039.
50 F. Neese, *WIREs Comput Mol Sci*, 2012, **2**, 73–78.
51 F. Weigend and R. Ahlrichs, *Phys. Chem. Chem. Phys.*, 2005, **7**, 3297–3305.
52 J. Dunning, Thom H., *J. Chem. Phys.*, 1989, **90**, 1007–1023.
53 E. Wirnhier, M. Döblinger, D. Gunzelmann, J. Senker, B. V. Lotsch and W. Schnick, *Chem. Eur. J.*, 2011, **17**, 3213–3221.
54 M. Deifallah, P. F. McMillan and F. Corà, *J. Phys. Chem. C*, 2008, **112**, 5447–5453.
55 F. Caruso, M. Dauth, M. J. van Setten and P. Rinke, *J. Chem. Theory Comput.*, 2016, **12**, 5076–5087.
56 D. Jacquemin, B. Mennucci and C. Adamo, *Phys. Chem. Chem. Phys.*, 2011, **13**, 16987–16998.
57 M. J. van Setten, F. Caruso, S. Sharifzadeh, X. Ren, M. Scheffler, F. Liu, J. Lischner, L. Lin, J. R. Deslippe, S. G. Louie, C. Yang, F. Weigend, J. B. Neaton, F. Evers and P. Rinke, *J. Chem. Theory Comput.*, 2015, **11**, 5665–5687.
58 S. Grimme and F. Neese, *J. Chem. Phys.*, 2007, **127**, 154116.
59 D. Jacquemin, A. Planchat, C. Adamo and B. Mennucci, *J. Chem. Theory Comput.*, 2012, **8**, 2359–2372.
60 D. Jacquemin, I. Duchemin, A. Blondel and X. Blase, *J. Chem. Theory Comput.*, 2016, **12**, 3969–3981.
61 S. C. Yan, Z. S. Li and Z. G. Zou, *Langmuir*, 2009, **25**, 10397–10401.
62 G. Vile, D. Albani, M. Nachtegaal, Z. Chen, D. Dontsova, M. Antonietti, N. Lopez and J. Perez-Ramirez, *Angew. Chem. Int. Ed.*, 2015, **54**, 11265–11269.
63 R. Czerw, M. Terrones, J.-C. Charlier, X. Blase, B. Foley, R. Kamalakaran, N. Grobert, H. Terrones, D. Tekleab, P. M. Ajayan, W. Blau, M. Rühle, and D. L. Carroll, *Nano Lett.*, 2001, **1**, 457–460.
64 J. Yang, D. Wang, H. Han and C. Li, *Acc. Chem. Res.*, 2013, **46**, 1900–1909.
65 Y. Yu, S.-Y. Huang, Y. Li, S. N. Steinmann, W. Yang and L. Cao, *Nano Lett.*, 2014, **14**, 553–558.
66 F. Hüser, T. Olsen and K. S. Thygesen, *Phys. Rev. B*, 2013, **88**, 245309.
67 R. Ganatra and Q. Zhang, *ACS Nano*, 2014, **8**, 4074–4099.
68 M. D. J. Quinn, N. H. Ho and S. M. Notley, *ACS Appl. Mater. Interfaces*, 2013, **5**, 12751–12756.
69 (*a*) G. Pacchioni and H. Freund, *Chem. Rev.*, 2012, **113**, 4035–4072; (*b*) M. Sterrer, M. Heyde, M. Novicki, N. Nilius, T. Risse, H.-P. Rust, G. Pacchioni and H.-J. Freund, *J. Phys. Chem. B*, 2006, **110**, 46–49.
70 (*a*) L. Yang, M. L. Cohen and S. G. Louie, *Nano Lett.*, 2007, **7**, 3112–3115; (*b*) Q. H. Wang, K. Kalantar-Zadeh, A. Kis, J. N. Coleman and M. S. Strano, *Nat. Nano*, 2012, **7**, 699–712.
71 (*a*) A. Panda, C. K. Renshaw, A. Oskooi, K. Lee and S. R. Forrest, *Phys. Rev. B*, 2014, **90**, 045303; (*b*) X.-F. He, *Phys. Rev. B*, 1991, **43**, 2063–2069.
72 C. Merschjann, S. Tschierlei, T. Tyborski, K. Kailasam, S. Orthmann, D. Hollmann, T. Schedel-Niedrig, A. Thomas and S. Lochbrunner, *Adv. Mater.*, 2015, **27**, 7993–7999.
73 Y. Zhang, J. Liu, G. Wu and W. Chen, *Nanoscale*, 2012, **4**, 5300–5303.